Williamsburg, Virginia
ACTIVE 04
2004 September 20-22

Feedback Control of a Morphing Chevron for Takeoff and Cruise Noise Reduction

R.H. Cabell
NASA Langley Research Center
Mail Stop 463
Hampton, Va 23681

N. Schiller
National Institute of Aerospace
144 Research Drive
Hampton, VA 23666

J.H. Mabe, R.T. Ruggeri, G.W. Butler
The Boeing Company
PO Box 3707
Seattle, WA 98124-2207

ABSTRACT

Noise from commercial high-bypass ratio turbofan engines is generated by turbulent mixing of the hot jet exhaust, fan stream, and ambient air. Serrated aerodynamic devices, known as chevrons, along the trailing edges of a jet engine primary and secondary exhaust nozzle have been shown to reduce jet noise at takeoff and shock-cell noise at cruise conditions. Their optimum shape is a finely tuned compromise between noise-benefit and thrust-loss. The design of a full scale Variable Geometry Chevron (VGC) fan-nozzle incorporating Shape Memory Alloy (SMA) actuators is described in a companion paper. This paper describes the development and testing of a proportional-integral control system that regulates the heating of the SMA actuators to control the VGC's tip immersion. The VGC and control system were tested under representative flow conditions in Boeing's Nozzle Test Facility (NTF). Results from the NTF test which demonstrate controllable immersion of the VGC are described. The paper also describes the correlation between strains and temperatures on the chevron with a photogrammetric measurement of the chevron's tip immersion.

1. INTRODUCTION

Jet exhaust is a dominant noise source in modern turbofan engines. Past research has demonstrated a noise reduction benefit by putting tabs or chevrons on the fan and core nozzles of a turbofan engine to promote mixing between the flows at the engine exit [1]. For example, reference [1] demonstrated that reductions of over 2.5 EPndB could be obtained with different chevron configurations with only a small thrust loss. In general, the noise reduction benefit due to chevrons is believed to outweigh the economic penalty due to thrust loss, although more work is needed to better understand the chevron noise reduction mechanism [2]. Chevrons are also believed to reduce shock-cell noise at cruise through a similar mixing mechanism. Unfortunately, it is difficult to study chevrons for shock-cell noise due to the difficulty reproducing the required test conditions in ground facilities.

In anticipation of a flight test in the summer of 2005, Boeing developed a full-scale, movable chevron for the fan nacelle of a turbofan engine. The chevron will be used in conjunction with microphones on the aircraft fuselage to measure shock cell noise as a function of the chevron's immersion into the bypass flow of the engine. The movable chevron is based on the Variable Geometry Chevron (VGC) concept [3], which relied on shape memory alloy (SMA) actuators to morph the chevron into the bypass flow at takeoff and out of the flow at cruise. This morphing behavior was achieved using the ability of SMA actuators to convert thermal energy into mechanical energy. For the present work, heaters were installed on the SMA material to provide a means to externally control the chevron's immersion. The resulting concept is called a Powered VGC, or PVGC.

The PVGC requires a control system to heat the SMA and move the chevron to specified immersions. A feedback control system was used to regulate heating of the SMA to ensure accurate, repeatable chevron immersion in the presence of significant uncertainties in material properties and environmental conditions. These uncertainties include large variations in the ambient temperature and in the nozzle pressure ratio of the engine.

The PVGC design was recently tested in the Nozzle Test Facility (NTF) at Boeing Field in Seattle, Washington. The NTF produces heated bypass and cooled ambient flows over the chevron to simulate the thermal and aerodynamic loads encountered in flight. This paper describes the feedback control system used to control heating of the SMA and thereby precisely control the position of the chevron's tip. Tests were conducted to demonstrate controlled movement of the chevron to different tip locations at various flow conditions, and to demonstrate holding the chevron immersed

in the bypass flow while the nozzle pressure ratio changed. A technique was developed to estimate the chevron's tip location from strain measurements, since this will be required for the flight test. The technique used a linear model to relate strain and temperature measurements on the chevron with the chevron's tip location. The estimated tip location was used by the feedback control system during the closed loop tests, thereby demonstrating strain-based, closed loop control of a morphing structure.

The paper begins with a brief description of the PVGC test coupon used in the NTF test. The PVGC design is described in more detail in a companion paper [4]. A proportional-integral feedback control algorithm was used to control the tip immersion, and is described next. This is followed by a description of the linear model relating strains and temperatures with tip immersion. The results section includes a description of the test facility and test conditions. Open loop behavior of the chevron is described, followed by the results of closed loop control, including control to varying immersions at a fixed nozzle pressure ratio and maintaining a fixed immersion while nozzle pressure ratio was varied.

2. CONTROL APPROACH

This section describes the feedback control algorithm used to regulate tip immersion, and the linear model used to estimate tip immersion from strain and temperature measurements. The section begins with a brief description of the test article since that influenced the controller design. Readers are referred to the companion paper for a more detailed discussion of the design and construction of the PVGC [4].

A. Test Article

The PVGC design consists of shape memory alloy (NiTinol) bars mounted on a stiff carbon-fiber composite base structure. NiTinol is a shape memory alloy which exhibits variable stiffness and a shape memory effect depending on the thermomechanical history of the material [5]. It can produce high forces and large displacements in a compact actuator. The NiTinol bars were trained to adopt a curved shape at high temperature (corresponding to their austenitic state), so when attached to the composite base the bars applied a large bending force to the base. At low temperature, (in the martensitic state), the NiTinol bars flattened out, and the stiffness of the composite base returned the chevron to a flat profile. The temperature of the NiTinol bars was regulated by current supplied to electrical resistance heaters bonded to the NiTinol.

There are considerable design challenges in creating a composite substrate of proper stiffness and shape to produce the desired three-dimensional profile when mated with NiTinol in both the austenite and martensite states [4]. The stiffness of the substrate and NiTinol must be considered, as well as the trained shape of the NiTinol in its austenite condition. The transition temperatures of the NiTinol to and from the austenite and martensite states was an additional variable for the particular NiTinol composition used here. For these tests, the NiTinol was predominantly martensitic below $0°$C and predominantly austenitic above $60°$C.

B. Feedback Control System

A feedback control system was used to regulate the tip immersion of the chevron. Feedback control was deemed to be the best way to produce repeatable tip immersions in the presence of significant variations in temperature and aerodynamic loading on the chevron. The controller regulated the current sent to heaters attached to the NiTinol bars; cooling was assumed to be provided by air flowing over the chevron.

A variety of feedback control algorithms could be used, depending on requirements such as step response time, robustness to uncertainty, and computational complexity. Numerous applications of feedback control to SMA-actuated structures can be found in the references [6, 7, 8, 9]. Some works describe the incorporation of hysteresis models for SMA behavior in the controller to improve response time and tracking behavior [12]. A simple proportional-integral (PI) controller was selected for the PVGC since the control objective was stable, robust operation with minimum steady state error to a step input. The PI controller didn't require a complicated model of the chevron, or knowledge of the temperature and loading history of the SMA material. The results will illustrate that assuming a first order model of the chevron's dynamics, and thereby neglecting any nonlinearities, was sufficient to design a well-performing PI controller.

A block diagram of a continuous-time proportional-integral (PI) controller applied to a generic plant is shown in Fig. 1. The control signal is proportional to the error signal and the integral of the error signal as determined by the gains K_p and K_i/K_p. Either a large error or a large integrated error will result in a large control signal. The integral

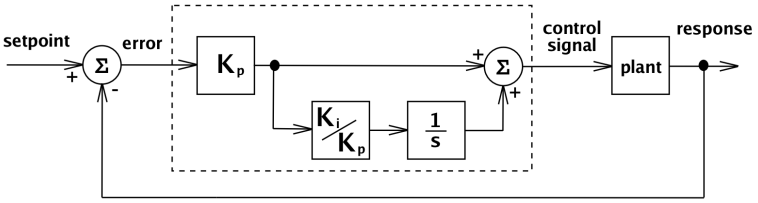

Figure 1: Block diagram of proportional-integral control system.

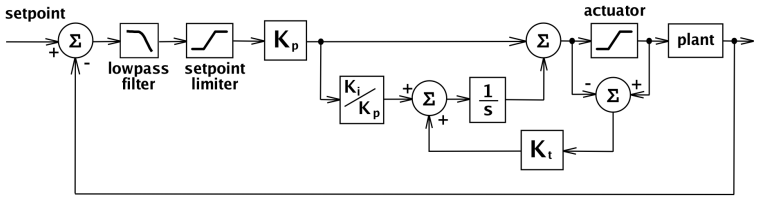

Figure 2: Proportional-integral control system with anti-windup.

term eliminates steady state error between the chevron's immersion and the desired immersion. A transfer function representation of the controller is written

$$H(s) = K_p \left(1 + \frac{K_i/K_p}{s}\right) \tag{1}$$

where K_p is the proportional gain and K_i/K_p is the integral gain. Tuning the controller requires choosing the location of the controller zero (K_i/K_p), and determining the overall controller gain, K_p.

An added complexity in the chevron application is due to the physical limits of the heaters on the NiTinol bars. The heaters can dissipate a limited amount of heat before burning up, which limits the maximum control current. In addition, the minimum control current is 0 Amps, since no active cooling was used. This means the control signal must saturate at a maximum and minimum current, which in turn can result in integrator windup [10]. The integrator in the controller will windup to very large values when an error exists between the setpoint and measured plant response and the actuator is saturated. When this occurs, the plant response will tend to over- or undershoot a setpoint. Setpoint limiting and back-calculation were used to limit the effects of integrator windup. Setpoint limiting, indicated by the saturation block on the left side of the block diagram in Fig. 2, limits the maximum error entering the control system. This can reduce integrator windup, but it can lead to conservatism in controller performance [10]. Back-calculation involves a second feedback signal defined as the difference between the control signal and the actuator output. This signal is zero when the actuator is operating in the linear range. When the actuator saturates, the difference between the commanded and applied signal is fed back to the integrator, thereby limiting the integrator's input. The diagram also shows a lowpass prefilter, which was used to reduce high frequency noise which could saturate the digital to analog converter in the control system.

C. Estimation of Tip Immersion

Another objective of the NTF test was to develop a method to estimate chevron immersion in a manner suitable for use on the flight test. During the NTF test, a photogrammetry system, described later in this paper, provided real-time (1 Hz) measurements of tip immersion, but such a system would not be practical for every chevron during the flight test. Hence, a method was devised to estimate immersion from strains and temperatures on the composite substrate. Although strains may be sufficient to predict tip immersion, temperatures were included to compensate for any temperature-induced output of the strain gages. This estimate was used as the tip immersion measurement for closing the loop in the feedback control system.

The linear relationship between strains, temperatures, and tip immersion was assumed to be of the form

$$z(n) = \beta_0 + \beta_1 t_1(n) + \beta_2 t_2(n) + \ldots + \beta_k s_1(n) + \beta_{k+1} s_2(n) + \ldots \tag{2}$$

Figure 3: Chevron during final assembly.

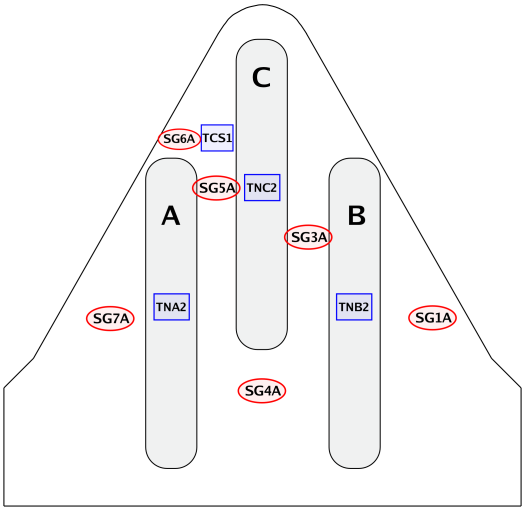

Figure 4: Instrumentation locations.

where $z(n)$ is the location of the chevron's tip along an axis perpendicular to the stream-wise direction, and $t_1(n)$ denotes the output of temperature sensor 1 at time n, and $s_1(n)$ denotes the output of strain sensor 1 at time n. No derivatives of strains, temperatures, or other state variables were used in the model, which is equivalent to assuming the chevron was at equilibrium at every time step, n.

Linear regression was used to compute the coefficients (β_i) in the model from calibration data [11, Chapter 2]. The calibration data consisted of discrete-time measurements of strains, temperatures, and tip immersions. The accuracy of this approach depends on which strains and temperatures are included in the model, and whether the calibration data is collected at representative operating conditions. A further constraint is that the model should use as few measurements as possible to simplify flight-test implementation. Data from the NTF test were used to select a subset of strains and temperatures from a larger candidate set, and to study the sensitivity of the model to tunnel operating conditions. This information will be used to design a calibration procedure for the flight article.

3. EXPERIMENTAL SYSTEM DESCRIPTION

A. Powered VGC Test Coupon

The powered variable geometry test coupon consisted of three basic parts: a stiff carbon-fiber substrate, NiTinol bars bolted to the substrate to provide bending forces, and a flexible fiberglass cover over the NiTinol bars to maintain smooth flow over the chevron. The companion paper [4] has more details on this design, which was based on a previous design discussed in reference [3]. A photo of the PVGC during final assembly is shown in Fig. 3. The photo shows three NiTinol bars lying on top of the carbon fiber substrate; the fiberglass cover has not yet been attached to the chevron. The side of the chevron visible in the photo is the side that will face the free stream in the tunnel test. The substrate is attached to an aluminum flange, visible in the top of the photo, for mounting to the wind tunnel. The base of the substrate had a radius of curvature of 121 cm, corresponding to the radius of curvature of a turbofan engine nacelle.

After the photo was taken, instrumentation and electrical resistance heaters were added to the NiTinol bars and the substrate. Figure 4 shows the locations of six strain gages mounted on the substrate, identified by labels such as SG1A, and four thermocouples, three of which were on the NiTinol bars. The strain gages were placed in areas of maximum bending strain due to activation of the NiTinol bars, and in areas sensitive to bending effects due to aerodynamic loading of the chevron. Additional strain and temperature gages were mounted on the chevron, but only those shown in the figure were acquired by the feedback control system.

Six electrical resistance heaters were attached to the top of each NiTinol bar (the side visible in the photo in Fig. 3). The heaters on a NiTinol bar were wired in a series-parallel combination and powered by a voltage-controlled power supply. The output current of the supply was proportional to an input voltage computed by the feedback control

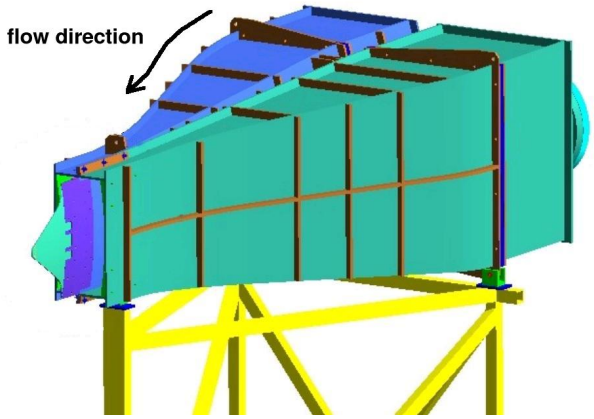

Figure 5: Converging hot and cold stream nozzles in nozzle test facility.

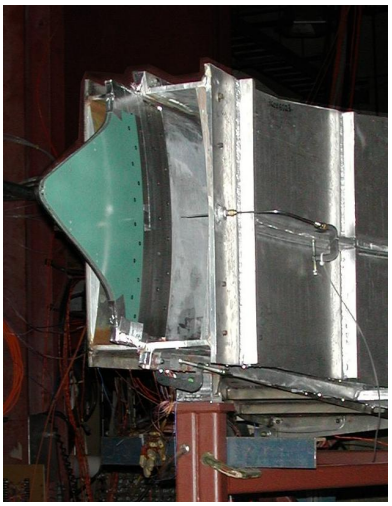

Figure 6: Photo of chevron at nozzle exit.

system. Each NiTinol bar had its own power supply, although nominally they were driven with the same control signal. Slight adjustments were made to the control signals going to each power supply to account for different heat flow rates from the NiTinol bars. In the flight test, the NiTinol bars will probably be driven by a single power supply to minimize complexity. The NiTinol was not actively cooled, but significant passive cooling was present due to heat conduction to the substrate and fiberglass cover, whose temperatures were closely coupled with the fan and free stream flows.

B. Nozzle Test Facility

The VGC coupon was tested in Boeing's Nozzle Test Facility (NTF). This facility provides independent hot and cold streams to simulate the fan and free stream flows over the chevron. The NTF has a 20 kg/sec flow capacity, which for this test was diverted into two controlled streams, one for the hot side and one for the cold side. The hot side is heated with a propane burner capable of heating an 18 kg/sec flow to 120° C. On the cold side, a liquid nitrogen (LN2) coolant is sprayed into the air flow via atomizing nozzles. The cold side can deliver 11 kg/sec of nitrogen rich air at a total temperature of -43° C. The thermally conditioned hot and cold air streams flow into a measurement station where total temperatures and pressures are obtained. From there, the flows go through showerhead nozzles into independent settling chambers, and are then accelerated through 8:1 contraction ratio nozzles. These contracting nozzles are shown in Fig. 5, with a viewpoint looking upstream, where the hot and cold nozzle exits are at the lower left of the figure, and the supply air enters at the upper right side of the figure. The flows pass over the test article and into the test cell, which vents to ambient.

The chevron test article was mounted at the exit of the contraction nozzles where the hot and cold streams converge, as shown in Fig. 6. The photo shows the free stream side of the chevron with the fiberglass cover. The tunnel attachment surface had a radius of curvature matching the nacelle curvature of a turbofan engine.

C. Photogrammetry Measurement System

A two-camera photogrammetry system measured the three dimensional locations of approximately 140 points on the chevron. Reflective dots were placed on the fan stream side of the chevron at each measurement point. The photogrammetry data were stored during each test and analyzed later to provide location data accurate to 0.03 mm. The photogrammetry system also provided a raw measurement of the chevron's tip position which was not as accurate as the post-processed data, but was available at a 1 Hz rate. This raw measurement was used for initial calibration of the strain-tip immersion model. A more thorough correlation of strains to tip measurements was done after the tunnel test once the photogrammetry data had been post-processed.

To compensate for movement of the tunnel structure, the chevron's tip immersion was defined relative to a point on the base of the chevron. The zero immersion point was defined where the body of the chevron was parallel to the

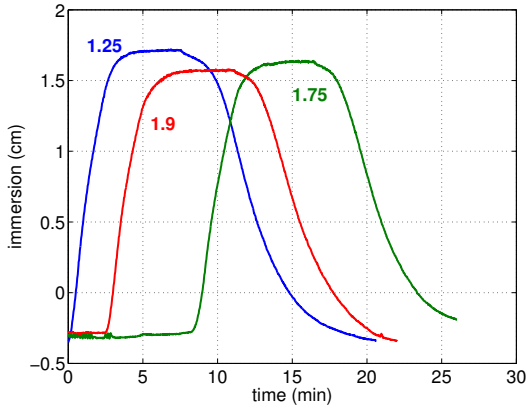

Figure 7: Tip immersion for three nozzle pressure ratios.

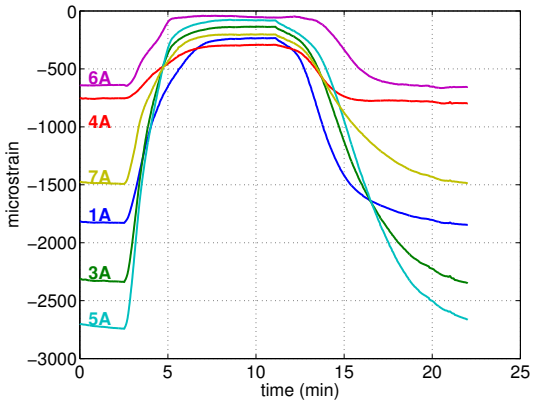

Figure 8: Strains for NPRH=1.9.

hot and cold stream flows. When the NiTinol was in its martensite state, the test coupon deflected slightly into the cold stream, resulting in a negative tip immersion.

4. RESULTS

VGC testing was conducted in the NTF facility during the first two weeks of April, 2004. Nearly 60 runs were conducted using two composite substrates of different stiffnesses. Results are presented here for the second of the two tested substrates, which was the less stiff of the two. No significant differences in terms of control design or closed loop behavior were seen between the two substrates.

A. Test conditions

Tests were conducted at conditions simulating takeoff and cruise temperatures and nozzle pressure ratios. Certain runs started at takeoff conditions, transitioned to cruise, then returned to takeoff, to subject the chevron to environmental variations seen in flight. Cruise conditions are most relevant for feedback control since temperatures at takeoff are too high to allow the NiTinol to become fully martensitic. The results reported here were all measured with the tunnel simulating cruise conditions. At cruise, the total temperature on the hot side was $\approx 15°$C while the cold side was $-40°$C. The hot side nozzle pressure ratio (referred to as NPRH) varied from 1.05 to 1.9, while the cold side was maintained at a pressure ratio of approximately 1.05.

B. Open loop operation

Open loop step responses were collected at three different NPRH values with the hot and cold side temperatures set to cruise conditions. These step responses characterized the dynamics of the PVGC and provided calibration data for the tip estimation model. A current of 3.5 A was applied to the heaters until the NiTinol center-point temperatures reached about $60°$C, at which point the current was reduced to maintain the NiTinol temperatures at $\approx 80°$C. Figure 7 shows time histories of tip immersion, in centimeters, for nozzle pressure ratios (NPRH) of 1.25, 1.75, and 1.9. The data consist of post-processed measurements from the photogrammetry system. The chevron started each run immersed in the free stream by 0.3cm, then moved into the fan stream 1.55cm to 1.70cm, depending on the nozzle pressure ratio, for a total tip excursion of $\approx$ 2cm. Maximum tip immersion was inversely related to NPRH, although the tip immersion was only 0.15cm greater at NPRH=1.25 than at NPRH=1.9. The heating time constant was about 120 seconds, and the cooling time constant was about twice that. The response is primarily 1st order, which makes sense for a system dominated by thermal effects.

Figure 8 shows time histories of strains for the NPRH=1.9 case. The curves are labeled corresponding to the instrumentation labels in Fig. 4. Zero strain for each gage was defined as the strain produced when the NiTinol was fully austenitic with no tunnel flow, corresponding to maximum deflection of the chevron. The curves in the figure indicate the strains did not reach this zero point at this nozzle pressure ratio. The largest change in strain occurred

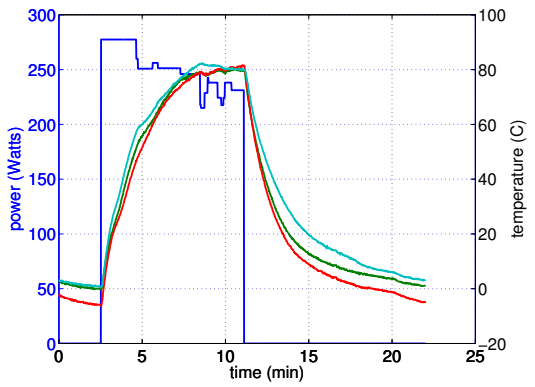

Figure 9: Heater power and NiTinol temperature for NPRH=1.9.

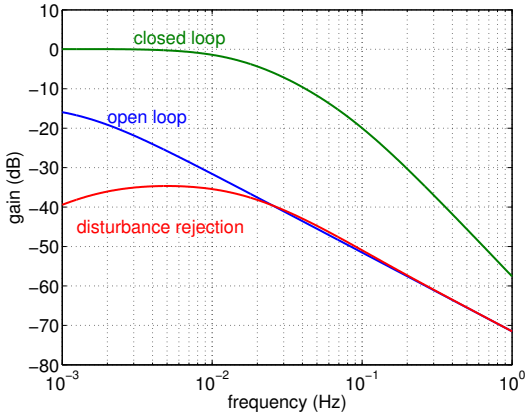

Figure 10: Open and closed loop transfer functions.

at gages 3A and 5A, near the midpoint of the center NiTinol bar, with the strain at location 5A increasing by nearly 2500 $\mu\epsilon$. Gage 4A, near the base of the chevron, and gage 6A, near the tip of one of the NiTinol bars, showed the smallest delta strain during the run.

The heater power and NiTinol temperatures for this run are shown in Fig. 9. The heater power is indicated by the stair step blue curve, which shows that a 275 Watts was applied at $t = 2.5$ minutes. The NiTinol temperatures, shown by the red, green, and light blue curves, reacted very quickly to the power input and began increasing from $0°$C. As the temperatures reached $80°$C the heater power was reduced to about 230 Watts (as commanded by an engineer in the loop). When power to the heaters was removed at $t = 11$min., the temperatures quickly dropped back to their starting points. The red temperature curve, corresponding to NiTinol bar B, indicates this bar was more closely coupled to the cold side than the other two bars. This bar fit more snugly into a slot in the tunnel mounting bracket than NiTinol bar A, resulting in greater heat loss to the surrounding structure.

C. Closed loop operation

This section describes closed loop operation of the PVGC, including immersing the chevron to specific setpoints, and maintaining a setpoint while the nozzle pressure ratio was changed. The section starts by describing the assumed plant model, the control gains, and the coefficients of the strain to tip immersion model.

The open loop chevron responses were predominantly first order, so a first order model was assumed for the PVGC plant, from current input to tip location. Based on the open loop data, a continuous time model was defined as

$$G(s) = \frac{0.4}{120s + 1} \tag{3}$$

This simple model neglects several aspects of the true relationship between applied current and chevron tip immersion, such as temperature-displacement hysteresis in the NiTinol. This hysteresis means the tip location is not a unique function of the temperature of the NiTinol. The model also neglects the squared relationship (i.e., non-linear) between heat energy produced by the resistance heaters and input current. It also assumes a linear relationship between NiTinol heating and tip immersion, which may not be accurate if the composite substrate snaps through due to its compound curvature.

In spite of these assumptions, the first order model was assumed to be accurate enough given the robustness of a proportional-integral controller [10]. Non-linearities and neglected properties mentioned in the preceding paragraph could be treated as uncertainties in the time constant of the chevron model, which could reduce the closed loop performance. If the control algorithm were able to completely capture the previously mentioned VGC characteristics, the step response time and closed loop bandwidth might be improved. However, it was assumed that adding such terms to the model and controller would provide a small benefit in this low-bandwidth application for a corresponding large increase in controller complexity.

Based on the first order chevron model in Eq. 3, the controller gain K_p was set to 50, and K_i/K_p was set to 0.01. The corner frequency of the first order lowpass filter was set to 0.1 Hz. The pole of this filter had little affect

Parameter Name	Coefficient Value
SG3A	$3.12e-7$
SG4A	$6.15e-4$
SG5A	$1.96e-4$
SG7A	$1.16e-5$
TCS1	$-3.5e-3$
β_0	0.9

Table 1: Parameters used in model to predict tip immersion

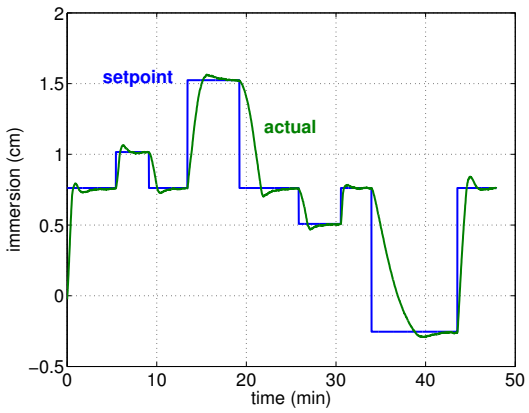

Figure 11: Closed loop control.

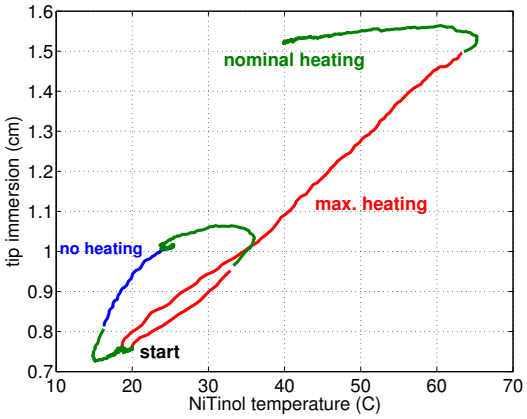

Figure 12: Temperature/tip immersions hysteresis.

on the transient response of the system because its dynamics were an order of magnitude faster than the plant. The back-calculation gain was set to 0.01. The saturation block at the output of the controller allowed a maximum current of 3.5 Amps and a minimum current of 0 Amps. The error-limiting saturation block at the input to the controller saturates at a maximum error of 3.5 and a minimum error of -1. In hindsight, the error-limiting values were probably too large since the maximum error was always less than 2cm. Neglecting the saturation blocks, the open and closed loop transfer function from setpoint input to tip immersion are shown in Fig. 10, assuming a first order chevron model. Closing the loop increases the system bandwidth by more than a factor of 10, and reduces the steady state error to zero. In practice, the saturation blocks will limit the speed of the closed loop step response, but if the control signal stays within the saturation limits, the curves in the figure give some idea of the increased bandwidth due to closing the loop.

The red curve in the figure shows how the controller will reject disturbances which enter at the input to the actuator. The curve indicates the closed loop system will reject very low frequency disturbances which could move the chevron's tip from its desired location. Although the actuator input is an unlikely path for disturbances, the curve provides some idea of disturbance rejection for paths similar to the NiTinol heating path. An example might be changes in heat loss due to conduction to the composite substrate when the temperature of either the fan or free stream flow changes.

Although a near real-time measurement of tip immersion was available from the photogrammetry system, the strain-tip immersion model was used as the measurement in the control system. A cursory look at the uncorrected photogrammetry data suggested that 4 strains and the temperature of the composite substrate (TCS1) would be useful parameters for the model. Data from the open loop run at NPRH=1.25 were used as calibration data for computing the coefficients of the model, which are listed in Table 1. The coefficients indicate that tip immersion was positively correlated with the four strains, and negatively correlated with the substrate temperature. The small coefficient for SG3A indicates that strain could probably be left out of the model with negligible effect. The R^2 value [11] for the linear regression was greater than 99%, indicating that the model explained more than 99% of the variation in the calibration data set.

Figure 11 shows closed loop results when the tip immersion was driven to specified values while the nozzle

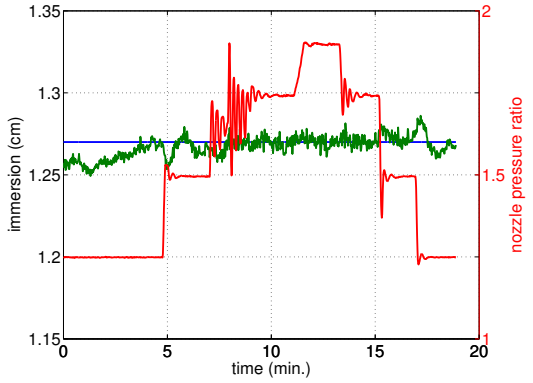

Figure 13: Holding setpoint while NPRH varied.

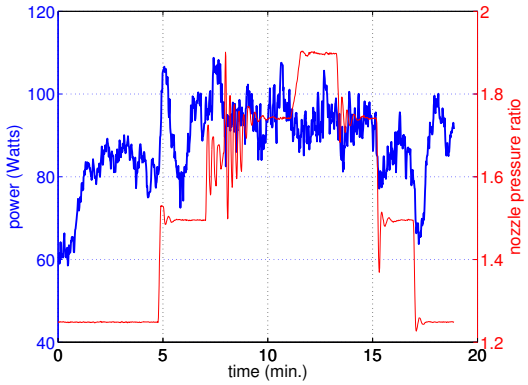

Figure 14: Heater power while NPRH varied.

pressure ratio (NPRH) was held at 1.25. The stair-step blue curve shows the commanded tip immersion, while the green curve shows the tip immersion as computed by the 5 parameter model in Table 1. The results show good closed loop performance, with some overshoot of the setpoint when heating and some undershoot when cooling. Some of this over- and undershoot was a result of integrator windup, and it could probably be reduced by more careful tuning of the back-calculation gain or the error-saturation limits.

To illustrate temperature-displacement hysteresis in the NiTinol, the center-point temperature of NiTinol bar B is plotted vs. tip immersion, for $t = 4$ to $t = 19$ min. of the run, in Fig. 12. The start label in the figure indicates the starting point of the data at $t = 4$ min., at a tip immersion of 0.76 cm. When the setpoint was changed to 1 cm, the feedback controller commanded maximum heating of the NiTinol, as indicated by the red portion of the curve. This raised the NiTinol's temperature from 21°C to 32°C, at which point the controller reduced the current, while the tip immersion increased to 1 cm. After the reduction in current, the NiTinol temperature decreased while tip immersion increased, before settling down to 1 cm at 24°C. The setpoint was then dropped back to 0.76 cm and the controller turned off the heaters, indicated by the blue portion of the curve. Heat was turned back on as the immersion approached the setpoint, but the immersion undershot the setpoint before rising back and returning to the start position. When the setpoint was increased to 1.52 cm, the controller commanded maximum power, increasing the temperature of the NiTinol from 21°C to nearly 65°C. Once again the immersion overshot the setpoint, and the controller applied only nominal heating while the NiTinol temperature dropped to 40°C to hold the immersion at 1.52 cm. The shape of the smaller hysteresis loop in relation to the larger loop is consistent with previous results where PID controllers were used on SMA-actuated structures [12].

Results from a second closed loop run where tip immersion was held constant while NPRH was varied are shown in Figure 13. The commanded setpoint was 1.27 cm, indicated by the blue line in the figure, while the achieved setpoint is indicated by the green line. The red curve shows NPRH, which started at 1.25, increased to 1.9 in three steps, and then dropped back to 1.25 during the run. The oscillations in NPRH near 1.75 were due to the tunnel flow control system, and were not related to the chevron. The green curve indicates the control system was able to hold the immersion constant while the nozzle pressure ratio varied. The corresponding heater power required to hold the tip immersion constant is shown in the blue curve in Fig. 14. Between 80 and 100 Watts were sufficient to maintain the tip immersion, and only small changes in power were needed as NPRH varied.

D. Accuracy of tip immersion estimate

The feedback results discussed so far involved closing the loop on tip immersion computed from a linear model of strains and temperatures. The weighting coefficients of the model were computed from a cursory analysis of open loop responses such as those shown in Fig. 7. This cursory analysis used uncorrected data from the photogrammetry system. Errors in the data were accepted since they were small, and didn't impact the goal of demonstrating feedback control using strain measurements.

Figure 15 compares three measurements of tip immersion for the closed loop run illustrated in Fig. 11: Corrected photogrammetry data; raw, uncorrected photogrammetry data; and estimated immersion computed during the NTF test using the linear model and coefficients listed in Table 1. The corrected and raw measurements agree to within

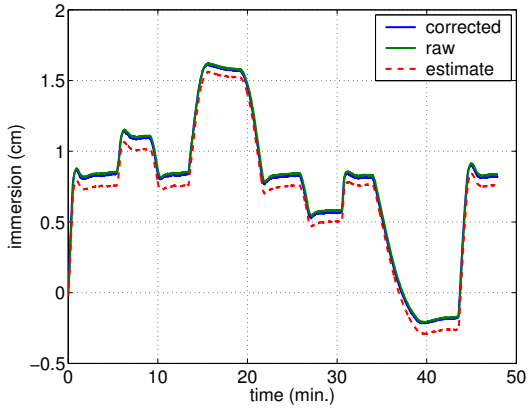

Figure 15: Corrected, raw, and estimated tip immersions.

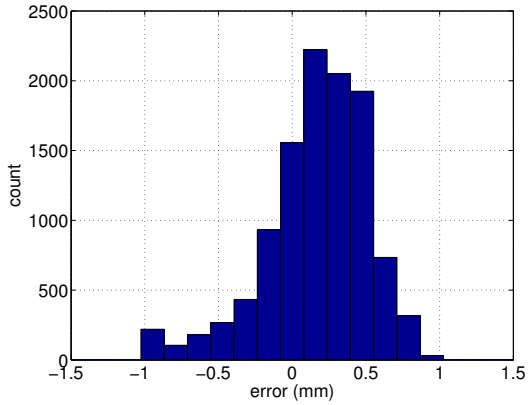

Figure 16: Histogram of errors for model using strains 6A and 7A.

0.5 mm for the entire run. The estimate is consistently below the corrected value, but the error is less than 1 mm for all but a few points during the run.

A more thorough analysis of parameters to include in the tip immersion model was done using the corrected photogrammetry data. The analysis considered which runs to use for calibration, which runs to use to evaluate the model, and which parameters to include in the model. Space constraints prevent a discussion of the entire analysis here, but the analysis revealed that a model using strains 6A and 7A was accurate to within 1 mm for a wide range of runs. The model was calibrated using open loop response data from a single run collected at cruise conditions and at a NPRH of 1.9. Calibrating using data collected at other NPRH values did not yield as accurate a model. The model was used to estimate tip immersions for 10968 data points collected during 7 test runs in the NTF. All of these runs were measured at cruise conditions, but the NPRH varied from 1.25 to 1.9. A histogram of the estimation errors is shown in Fig. 16. The error is the difference between the estimated and the corrected tip immersion. The histogram shows that over 80% of the errors were equal to or less than 0.5 mm.

5. CONCLUSIONS

Strain-based feedback control of a powered, variable geometry chevron was demonstrated in Boeing's Nozzle Test Facility. Actuation was provided by NiTinol bars bolted to a carbon-fiber composite base structure. Strain gages and thermocouples on the chevron were used to estimate the immersion of the chevron's tip into the fan stream side of the test facility. The feedback loop was closed using this tip immersion estimate. The results demonstrated that the chevron's tip could be regulated to tip immersions ranging from 0.25 cm into the free stream to 1.5 cm into the fan stream. The feedback controller was also able to maintain a tip immersion of 1.27 cm into the fan stream while the nozzle pressure ratio was varied from 1.25 to 1.9. A post-test analysis of tip immersions and strain data revealed that two strains were sufficient to estimate the tip immersion to within 1 mm accuracy.

REFERENCES

[1] Naseem H. Saiyed, Kevin L. Mikkelsen, and James E. Bridges. Acoustics and thrust of separate-flow exhaust nozzles with mixing devices for high-bypass-ratio engines. In *6th AIAA/CEAS Aeroacoustics Conference*, number AIAA-2000-1961, Lahaina, HI, June 2000.

[2] R.H. Thomas, K.W. Kinzie, and S. Paul Pao. Computationl analysis of a pylon-chevron core nozzle interaction. In *7th AIAA/CEAS Aeroacoustics Conference*, number AIAA-2001-2185, Maastricht, The Netherlands, May 2001.

[3] F.T. Calkins and G.W. Butler. Subsonic jet noise reduction variable geometry chevron. In *42nd AIAA Aerospace Sciences Meeting and Exhibit*, number AIAA-2004-0190, Reno, NV, January 2004.

[4] James H. Mabe, Robert T. Ruggeri, G.W. Butler, and Scott Sellmeyer. Morphing chevrons for takeoff and cruise noise reduction. In *Active 2004*, Williambsburg, VA, September 2004.

[5] K. Otsuka and C.M. Wayman, editors. *Shape Memory Materials*. Cambridge University Press, New York, 1998.

[6] Robert B. Gorbet, Kirsten A. Morris, and David W.L. Wang. Passivity-based stability and control of hysteresis in smart actuators. *IEEE Transactions on Control Systems Technology*, 9(1):5–16, January 2001.

[7] Daniel R. Madill and David Wang. Modeling and l2-stability of a shape memory alloy position control system. *IEEE Transactions on Control Systems Technology*, 6(4):473–481, July 1998.

[8] Marina L. Tharayil and Andrew G. Alleyne. Modeling and control for smart mesoflap aeroelastic control. *IEEE/ASME Transactions on Mechatronics*, 9(1):30–39, March 2004.

[9] M.H. Elahinia and M. Ahmadian. Stress-based sliding mode control of a rotary sma-actuated manipulator. In *SPIE 11th Annual International Symposium on Smart Structures and Materials*, page 78, San Diego, CA, March 2004.

[10] Karl J. Åström and Tore Hägglund. *PID Controllers: Theory, Design, and Tuning*. Instrument Society of America, 2nd edition, 1995.

[11] N.R. Draper and H. Smith. *Applied Regression Analysis*. John Wiley and Sons, 2nd edition, 1981.

[12] Sumiko Majima, Kazuyuki Kodama, and Tadahiro Hasegawa. Modeling of shape memory alloy actuator and tracking control system with the model. *IEEE Transactions on Control Systems Technology*, 9(1):54–59, January 2001.